Lawrence Berkeley National Laboratory
LBL Publications

Title
Polarization control at the microscopic and electronic structure observatory

Permalink
https://escholarship.org/uc/item/72c9t97s

Authors
Moser, Simon
Kilcoyne, David
Denlinger, Jonathan D
et al.

Publication Date
2019

DOI
10.1016/j.nima.2018.06.029

Peer reviewed

eScholarship.org Powered by the California Digital Library
University of California

Polarization control at the Microscopic and Electronic Structure Observatory

Simon Moser,[1] David Kilcoyne,[1] Jonathan D. Denlinger,[1] Roland J. Koch,[1] Chris Jozwiak,[1] Aaron Bostwick,[1] and Eli Rotenberg[1]

[1] *Advanced Light Source (ALS), Berkeley, California 94720, USA*

The new Microscopic and Electronic Structure Observatory (MAESTRO) at the Advanced Light Source (ALS) in Berkeley provides X-rays of variable polarization, produced by an elliptically polarized undulator (EPU), for angle resolved photoemission (ARPES) and photoemission electron microscopy (PEEM) experiments. The interpretation of photoemission data, in particular of dichroism effects in ARPES, requires the precise knowledge of the exact polarization state. Numerical simulations show that the first harmonics of the EPU at MAESTRO provides soft X-rays of almost 100 % on axis polarization. However, the higher harmonics as well as the downstream optical elements of the beamline, have a considerable impact on the polarization of the light delivered to the experimental end-station. Employing a simple reflective polarimeter, the polarization is characterized for variable EPU and beamline settings and the overall degree of polarization in the MAESTRO end-stations is estimated to be on the order of 83 %.

INTRODUCTION

Elliptically polarized undulators (EPU) at third generation synchrotron light sources have enabled experiments with tunable light polarization [1]. In particular, angle resolved photoemission (ARPES) experiments benefit tremendously from this additional control parameter as the photoemission cross-section is directly determined by the dipole selection rules, and thus by the state of light polarization. Consequently, ARPES with variable light polarization can be used today to determine the chirality, the orbital character, and the spin texture of electronic systems by dichroism experiments [2–13].

Usually, the polarization in an ARPES experiment is assumed to be close to its nominal specification value and not discussed within the scope of the data interpretation. However, as will be shown, the real polarization delivered to the experimental end-station typically differs from the nominal value, and can result in an incorrect evaluation and interpretation of the data. In particular, the nearly free electron final state model of photoemission predicts artifacts in ARPES dichroism as a result of such improper polarization [14]. The careful calibration of the polarization at the ARPES beamline is thus an important prerequisite to distinguish such artifacts from intrinsic dichroism. A thorough polarization calibration, however, is cumbersome and time consuming, and has been discussed only in a few cases [15–26].

The focus of this article is the light polarization at the new Microscopic and Electronic Structure Observatory (MAESTRO), beamline 7.0.2 of the Advanced Light Source, comprising *in situ* μARPES, nanoARPES and PEEM capabilities. First, we assess the polarization output of the EPU by realistic numerical simulations. It is shown that by selecting first harmonics radiation close to the beam axis, the degree of polarization can be tuned up to 100 %. However, the optical elements of the beamline, in particular the monochromator assembly (moving mirror and grating), introduce significant changes in polarization to the detriment of the measured data. Finally, by employing a simple reflective polarimeter to continuously measure the polarization state at MAESTRO, the overall degree of polarization is estimated to be around 83 %.

CHARACTERIZING POLARIZATION

To appropriately describe the photon beam polarization, we first define our coordinate system with the z-axis along the incoming light direction (the beam axis) and the electric field vector perpendicular in the xy-plane. The electric field vector $\boldsymbol{\epsilon}$ in Jones notation then is given by [27]

$$\boldsymbol{\epsilon} = \begin{pmatrix} \epsilon_x \\ \epsilon_y \\ 0 \end{pmatrix} . \quad (1)$$

To assess the state of polarization, it is useful to rewrite $\boldsymbol{\epsilon}$ in terms of the Stokes parameters, defined as

$$\boldsymbol{S} = \begin{pmatrix} S_0 \\ S_1 \\ S_2 \\ S_3 \end{pmatrix} = \begin{pmatrix} \epsilon_x^2 + \epsilon_y^2 \\ \epsilon_x^2 - \epsilon_y^2 \\ 2\Re(\epsilon_x \epsilon_y^*) \\ -2\Im(\epsilon_x \epsilon_y^*) \end{pmatrix} . \quad (2)$$

S_0 denotes the intensity of the light, S_1 describes the degree of linear horizontal (LH, along x, $S_1 = 1$) and vertical (LV, along y, $S_1 = -1$) polarization, S_2 describes the degree of linear diagonal polarization (along $\pm 45^\circ$ rotated axes $x = \pm y$, $S_2 = \pm 1$), and S_3 describes the degree of right circular (RC, $S_3 = 1$) and left circular (LC, $S_3 = -1$) polarization. The total degree of polarization, i.e. the portion of the light wave that is polarized, is defined as

$$\Pi = \frac{\sqrt{S_1^2 + S_2^2 + S_3^2}}{S_0} \leq 1 . \quad (3)$$

If the light beam is manipulated by an optical element, like a mirror or a polarizer, then the state of the outgoing polarization can be changed with respect to its ingoing state. This change can be described by a Müller matrix [28, 29]. The Stokes vector $\boldsymbol{S}_f$ of the outgoing beam is related to the Stokes vector $\boldsymbol{S}_i$ of the ingoing beam by a matrix transformation comprising an initial rotation of the polarization vector into

Electron Energy (GeV)	1.9	Energy Spread	0.0011		
Average Current (mA)	500	b_x (m)	24	a_x	0
Circumference	196.8054150	b_y (m)	5.8	a_y	0
Bunches	328	h_x (m)	0	$h_{x'}$	0
s_z (mm)	6	h_y (m)	0	$h_{y'}$	0
Peak Current (A)	19.9477	$1/g$ (mrad)	0.268947		
Natural Emittance (mrad)	2.03×10^{-9}	s_x (mm)	0.2191	$s_{x'}$ (mrad)	9.129×10^{-3}
Coupling Constant	0.015	s_y (mm)	0.01319	$s_{y'}$ (mrad)	2.274×10^{-3}
e_x (mrad) 2×10^{-9}	e_y (mrad) 3×10^{-11}	$gs_{x'}$	0.03394	$gs_{y'}$	8.456×10^{-3}

TABLE I. Storage ring parameters at the ALS used for SPECTRA simulations.

the reference frame of the optical element $\mathcal{R}(\alpha)$, followed by a Müller matrix describing the optical element itself, and a final back-rotation $\mathcal{R}(-\alpha)$ into the initial light beam's frame of reference, given by

$$\boldsymbol{S}_f = \mathcal{R}(-\alpha)\mathcal{M}\mathcal{R}(\alpha)\boldsymbol{S}_i \ . \tag{4}$$

The rotation of the polarization by an angle α around the z-axis is described by

$$\mathcal{R}(\alpha) = \begin{pmatrix} 1 & 0 & 0 & 0 \\ 0 & \cos(2\alpha) & \sin(2\alpha) & 0 \\ 0 & -\sin(2\alpha) & \cos(2\alpha) & 0 \\ 0 & 0 & 0 & 1 \end{pmatrix} , \tag{5}$$

whereas the Müller matrix describing light reflection on a flat surface is

$$\mathcal{M}(\beta) = \begin{pmatrix} \frac{1}{2}\left(r_p^2 + r_s^2\right) & \frac{1}{2}\left(r_p^2 - r_s^2\right) & 0 & 0 \\ \frac{1}{2}\left(r_p^2 - r_s^2\right) & \frac{1}{2}\left(r_p^2 + r_s^2\right) & 0 & 0 \\ 0 & 0 & r_p r_s \cos(\delta_p - \delta_s) & r_p r_s \sin(\delta_p - \delta_s) \\ 0 & 0 & -r_p r_s \sin(\delta_p - \delta_s) & r_p r_s \cos(\delta_p - \delta_s) \end{pmatrix} . \tag{6}$$

According to the Fresnel equations, the s-polarized part of the electric field at a light incidence of β with respect to the surface normal is reflected as

$$r_s e^{i\delta_s} = \frac{N_1 \cos\beta - \frac{\mu_1}{\mu_2}\sqrt{N_2^2 - N_1^2 \sin^2\beta}}{N_1 \cos\beta + \frac{\mu_1}{\mu_2}\sqrt{N_2^2 - N_1^2 \sin^2\beta}} , \tag{7}$$

whereas the p-polarized component is reflected as

$$r_p e^{i\delta_p} = \frac{N_2^2 \frac{\mu_1}{\mu_2}\cos\beta - N_1\sqrt{N_2^2 - N_1^2 \sin^2\beta}}{N_2^2 \frac{\mu_1}{\mu_2}\cos\beta + N_1\sqrt{N_2^2 - N_1^2 \sin^2\beta}} . \tag{8}$$

N_1 and N_2 are the complex indices of refraction and μ_1 and μ_2 are the magnetic permeabilities of vacuum and the mirror surface, respectively. Approximating $\mu_1 = \mu_2 = N_1 = 1$, the only photon energy dependent quantity which enters into consideration is N_2. The reflection of light at the mirror is accompanied by a relative change of amplitude r_s/r_p as well as by a phase shift $\delta_s - \delta_p$ for the s and p polarized light components. These relative changes of amplitude and phase ultimately change the state of polarization.

THEORETICAL CHARACTERIZATION OF THE EPU

Soft X-rays at MAESTRO are produced by an APPLE-II-type EPU with period length 70 mm and a total length of 1906.05 mm [1]. This insertion device in principle allows for full photon energy and polarization control [30, 31]. The magnetic field strength $|B|$, controlled by the undulator gap size, determines the photon energy. The magnetic field ratio B_x/B_y and phase $\arctan 2(B_x, B_y)$ is controlled by the relative shift of the horizontal and vertical magnet rows with respect to each other, the row phase EPU_z, and determines the polarization direction. In particular, the continuous variation of EPU_z across an entire magnet period continuously changes the polarization state from LV to LC to LH to RC and back to LV. However, due to a mutual coupling of the relative field strength and phase under normal EPU operation conditions, linear polarized light rotated $45°$ with respect to LH or LV ($S_2 = \pm 1$) cannot be obtained .

Before characterizing the state of polarization at MAESTRO experimentally, the theoretical performance of the EPU is addressed by numerical simulation employing the synchrotron radiation calculation code "SPECTRA" [32]. The storage ring parameters describing the properties of the electron beam used for the calculations are summarized in Table I.

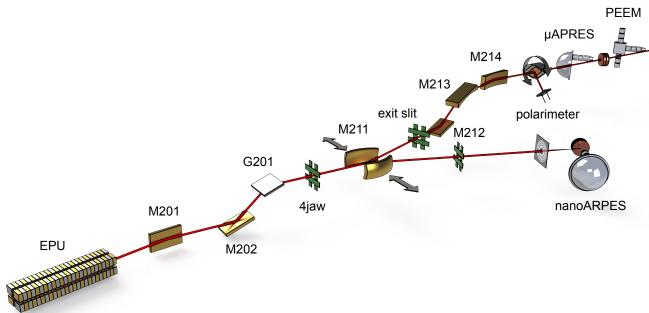

FIG. 1. Outline of the MAESTRO beamline [33].

Optimizing Photon Flux and Polarization

The EPU at MAESTRO produces an entire energy spectrum of soft X-rays, spatially distributed around the beam axis. A variable rectangular aperture (4jaw), about 15 m downstream of the EPU, limits the solid angle fraction of the light beam that is accepted into the beamline (Fig. 1). To maximize the photon flux and the degree of polarization at the same time, the width of the 4jaw needs to be carefully adjusted.

In Figure 2 the partial flux obtained for various acceptance angles imposed by the 4jaw is shown for both linear and circular polarized light. In the calculation, the first harmonics was set to 100 eV photon energy. For a small angular acceptance, i.e. a small 4jaw opening, primarily the on axis radiation is selected, which gives sharp harmonic contributions over the spectral range shown. In linear polarization, the even harmonic on axis contributions are quasi- suppressed. In circular polarization, all except the first harmonics on axis contributions are suppressed. Opening the 4jaw increases the acceptance angle and results in spectral tails towards the low energy side of all EPU harmonics.

Figure 3 shows the calculated degree of polarization for the transmitted light as a function of acceptance angle. Data is shown for gap parameters that set the first harmonics at 50 eV, 100 eV, and 150 eV in linear and circular polarization, respectively, for the first, second and third harmonics of the EPU. Theoretically, the degree of polarization is almost independent for acceptance angles below 1 mrad, and rapidly decreases once the 4jaw is opened further. The acceptance angle at which both photon flux as well as the degree of polarization are maximized depends on the position of the first harmonics (the gap of the EPU) and becomes smaller for higher energy first harmonics. This implies that in a fixed 4jaw configuration with fixed acceptance angle, the degree of polarization is expected to be lower at higher photon energies.

Figure 4 shows calculations of the partial flux as well as the degree of polarization for an optimized acceptance angle of 1 mrad. Results are again shown for the first harmonics at 50 eV, 100 eV and 150 eV in linear and in circular polarization, respectively. We observe that while the degree of polarization Π is almost ideal at the nominal energy position of the EPU harmonics, it rapidly decreases for energies above and below. This implies that EPU harmonics and monochromator assembly have to be carefully synchronized to guarantee a high degree of polarization over a wide photon energy range.

Intensity Distribution

Figure 5 shows the spatial intensity distribution at the 4jaw for the first, second and third harmonics in linear and circular polarized light configurations. The first harmonics is set to 100 eV. For linear polarization, the odd harmonics consist of s-type, whereas the second harmonics displays a two fold p_x-type intensity profile with a node on the y-axis, explaining the overall suppression of the second harmonics for small acceptance angles in Fig. 2. In circular polarization, the first harmonics again shows a simple s-type distribution. The higher orders, however, display donut like contours with on axis intensity nodes, responsible for the suppression of all higher harmonics at small acceptance angles in Fig. 2. These signatures are indicative of Laguerre-Gaussian modes with non-zero orbital angular momentum. As predicted in Refs. 34 and 35 and experimentally verified in Ref. 36, the orbital angular momentum l of an EPU harmonics n is then given by $l = n - 1$.

BEAMLINE PERFORMANCE

The optical path of the MAESTRO beamline comprises a series of optical elements such as mirrors and gratings, which deflect the X-ray beam from the upstream EPU to the downstream experimental end-stations (Fig. 1) [33]. Even though the effects of a single device are typically negligible, a series of such elements can cause sizable changes in the polarization [16, 20, 22, 37–39]. At MAESTRO, three fixed mirrors (M201,M211,M214) deflect the beam horizontally and two fixed mirrors (M212,M213) deflect the beam vertically. The deflection angles are given in Tab. II. The plane grating monochromator assembly consists of a gold mirror M202 moving conjointly with grating G201, keeping the beam vertically aligned when the photon energy is changed. The deflection angles of mirror and gratings for variable photon energies are shown in the top row of Fig. 6 for the four gratings available at MAESTRO.

M201	M202	G201	M211	M212	M213	M214
4.5°	$f(h\nu)$	$f(h\nu)$	4°	3°	3°	3°
h	v	v	h	v	v	h

TABLE II. Deflection angles and directions (h: horizontal, v: vertical) of the optical elements at MAESTRO

The effect of the grating on the polarization vector is not straightforward. Realistic models require a comprehensive solution of Maxwell's equations on the particular grating geometry, typically solved numerically by rigorous coupled-wave

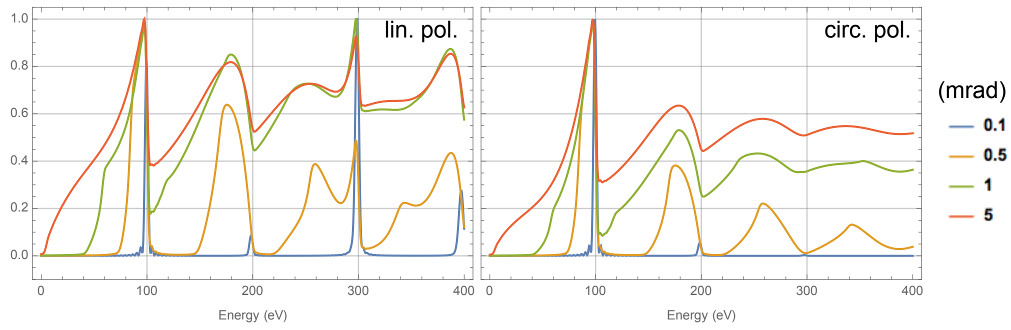

FIG. 2. Partial flux as a function of the acceptance angle imposed by the 4jaw. Calculations are shown for the linear (left) and circular (right) polarized EPU state. The first harmonics was set to 100 eV.

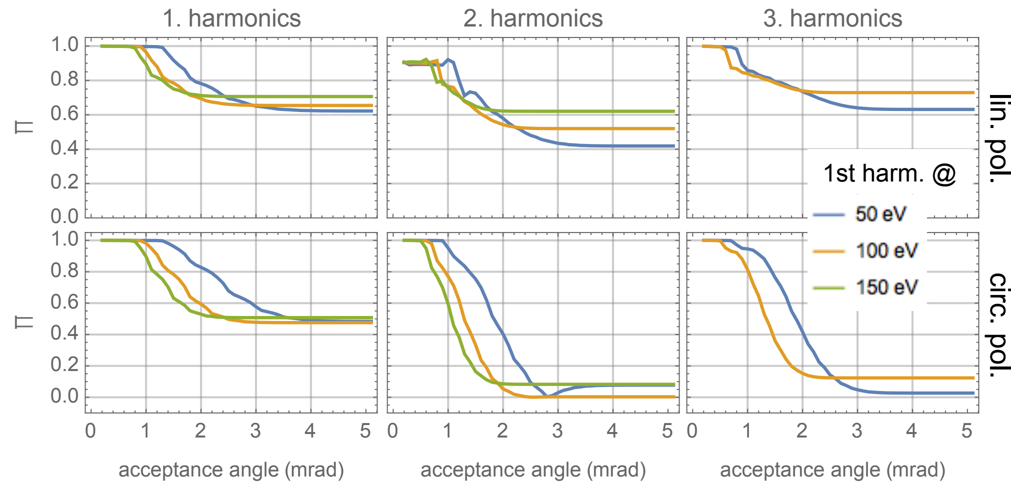

FIG. 3. Degree of polarization Π as a function of acceptance angle (4jaw opening) shown for linear (top) and circular (bottom) polarized EPU state. The first harmonics was set to 50 eV, 100 eV and 150 eV, respectively, and the degree of polarization is given for the first (left), second (middle), and third (right) harmonics, respectively.

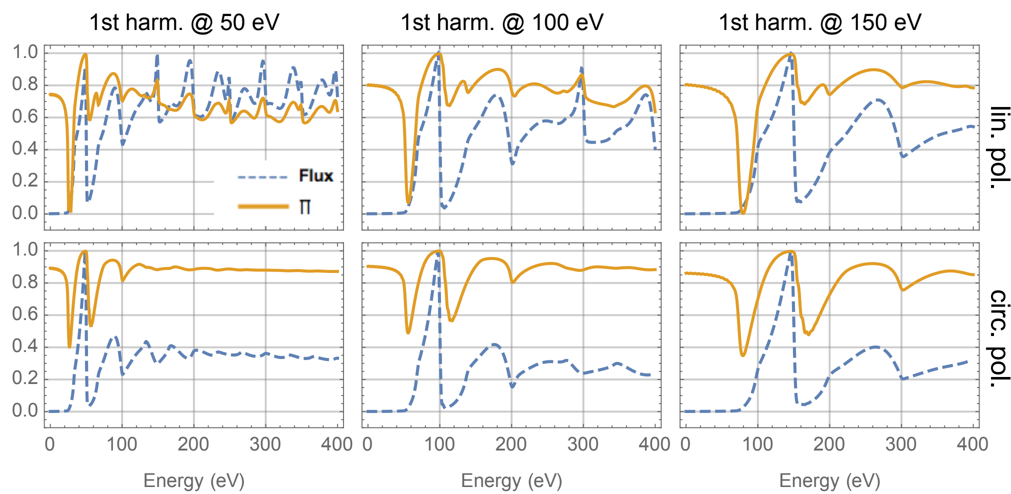

FIG. 4. Partial flux and degree of polarization Π as a function of photon energy calculated for an acceptance angle (4jaw opening) that optimizes the transmitted flux and degree of polarization of the first harmonics. Calculations are shown for the linear (top) and circular (bottom) polarized EPU state. The first harmonics was set to 50 eV (left), 100 eV (middle), and 150 eV (right), respectively.

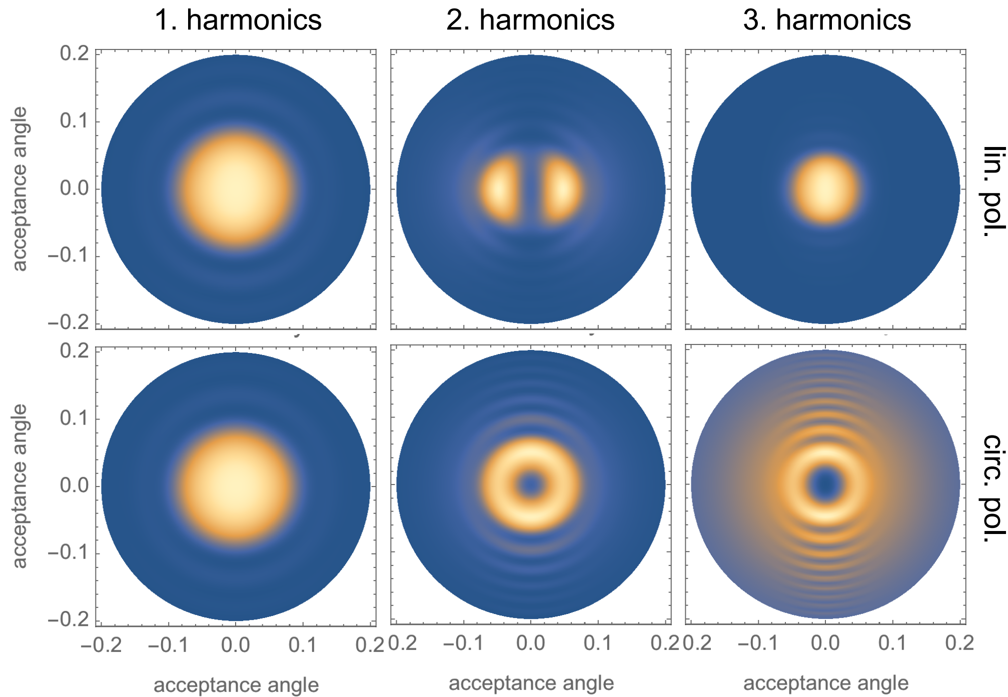

FIG. 5. Spatial intensity distribution of the first (left), second (middle), and third (right) harmonics for linear (top) and circular (bottom) polarized light. The first harmonics was set to 100 eV.

analysis [40–45], as implemented e.g. in software codes like "GSolver" or "Grating" [46]. Experimentally, this can be accomplished by Müller matrix polarimetry, a technique typically applied to characterize gratings in the optical regime [47–55]. To date, there has been no thorough theoretical study on how the grating affects polarization, and experimental studies are rather rare in the soft X-ray regime [38, 56–58].

A first order estimate for how the grating changes polarization can be obtained by an extremely simplified approach where all mirrors as well as the grating are modeled by Müller matrices that describe reflections from a plane surface [16]. At MAESTRO, all optical elements are coated with gold. Assuming the refractive index values tabulated for gold in Ref. 59, and employing equations 7 and 8, one can calculate the amplitudes r_s and r_p as well as the relative phase shift $\delta_s - \delta_p$ in between s and p polarized light components. The total Müller matrix transformation of the MAESTRO beamline is then given as

$$\begin{aligned}\boldsymbol{S}_f &= \mathcal{M}(\text{M214})\mathcal{R}(90°)\mathcal{M}(\text{M213})\mathcal{M}(\text{M212})\\ &\times \mathcal{R}(90°)\mathcal{M}(\text{M211})\mathcal{R}(90°)\mathcal{M}(\text{G201}, h\nu)\\ &\times \mathcal{M}(\text{M202}, h\nu)\mathcal{R}(90°)\mathcal{M}(\text{M201})\boldsymbol{S}_i\,.\end{aligned}$$

As this simplified model only accounts for coherent phase retardation in between s and p-polarized light components upon reflection, it describes the redistribution of spectral weight among S_1, S_2 and S_3, but leaves the total degree of polarization unchanged ($\Delta\Pi = 0$). This change of polarization as a function of photon energy is shown for all gratings available at MAESTRO in the middle and bottom row of Fig. 6. If the initial state of polarization is LH or LV, i.e. $|(S_0, S_1, S_2, S_3)| = (1, 1, 0, 0)$, then the principle light components are either purely s or p for all optical components and no dephasing effects occur (not shown). For $45°$ rotated linear polarized light $|(S_0, S_1, S_2, S_3)| = (1, 0, 1, 0)$ (middle row) and circular polarized light $|(S_0, S_1, S_2, S_3)| = (1, 0, 0, 1)$ (bottom row), with a mixture of s and p polarized light components, dephasing leads to significant changes of the initial polarization state. Due to smaller refraction angles of the monochromator assembly, these polarization changes become smaller for higher photon energies. At lower photon energies where the refraction angles at the monochromator assembly are large, however, the polarization can change by values well on the order of 5 to 15 %. Additionally, the actual grating can introduce sizable and nontrivial effects, which are not captured by this simplistic plane mirror model [53, 56, 57, 60].

POLARIZATION MEASUREMENTS

As previously discussed, the idealized EPU introduces fully polarized first harmonics X-rays into the beamline if the angular acceptance is sufficiently small. Dephasing at the optical components of the beamline, in particular at the monochromator assembly, can introduce sizable changes to the polar-

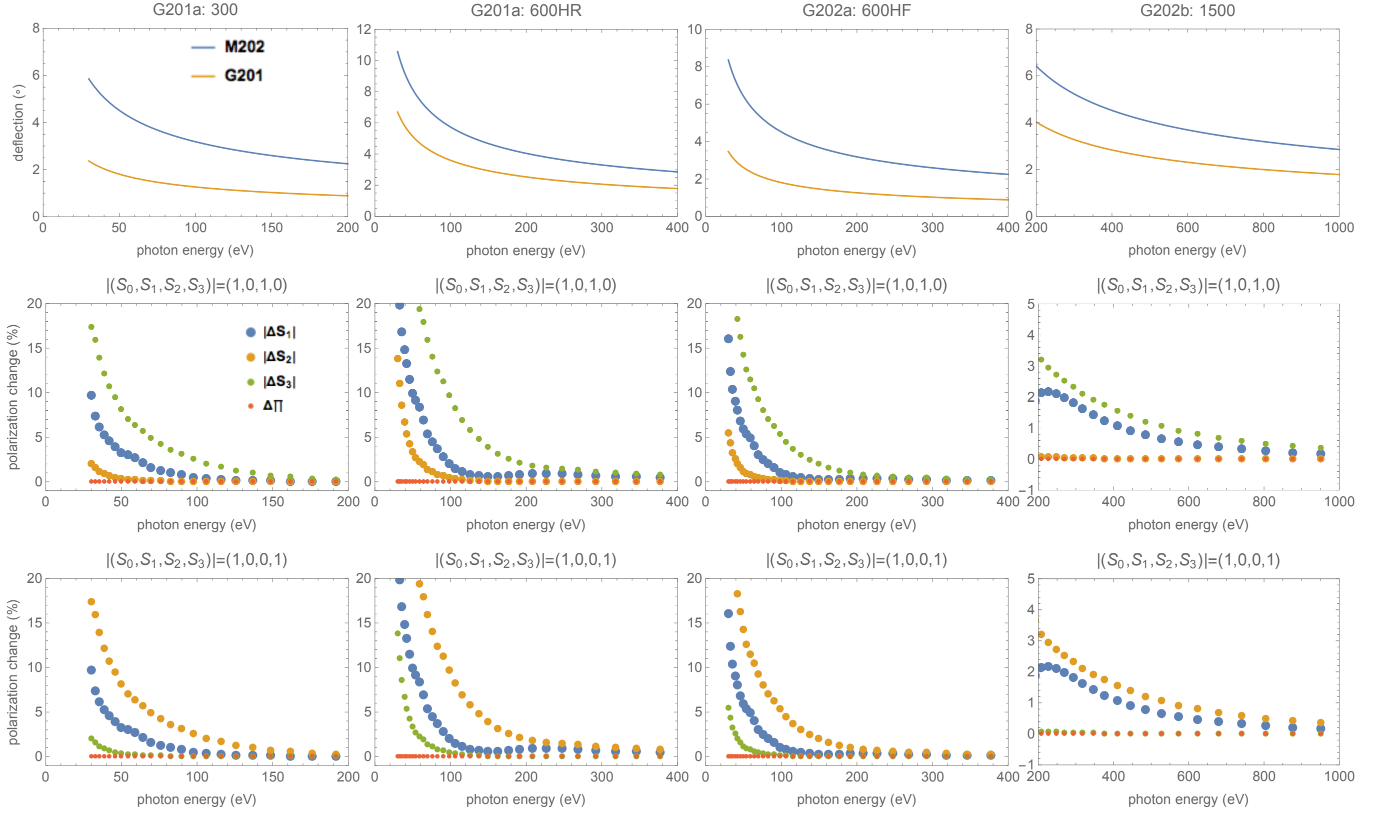

FIG. 6. Polarization change at the four monochromator assemblies G201a available at MAESTRO, with 300, 600 (HR: high resolution, HF: high flux), and 1500 lines per mm, respectively. The grating is modeled as a plane mirror. (top) Deflection angles of mirror M202 and grating G201. (middle) Polarization change for 45° linear polarized light ($|S_2| = 1$), not available at MAESTRO. (bottom) Polarization change for circular polarized light ($|S_3| = 1$). Polarization change for LH and LV polarized light ($|S_1| = 1$) is zero and therefore not shown.

ization state, but should leave the total degree of polarization ideally unaffected. In reality, both EPU as well as beamline optics exhibit imperfections. Incoherent light superposition at misaligned magnetic arrays, or incoherent scattering at rough or polluted optical components will thus lead to sizable depolarization effects that are difficult to assess theoretically [52]. Foremost, the diffraction condition for a given monochromator setting ($m/h\nu =$ const, m: diffraction order, $h\nu$: photon energy) is fulfilled for all EPU harmonics simultaneously, accepting a fraction of depolarized higher order EPU harmonics into the experimental end-station (see Fig. 4). It is thus appropriate to measure the polarization state close to the experimental end-station.

A full polarization characterization is typically obtained by ellipsometry, i.e. through a serial arrangement of polarizers and analyzers [28, 37, 61], but also less conventional methods based on photoelectron diffraction [62] or gas phase atomic/molecular polarimetry [63, 64] have been proposed. Here, a particularly simple reflective polarimeter is employed [39, 65–67], consisting of a gold mirror tilted by $\beta \sim 45°$ with respect to the incoming light axis (see Fig. 7). The light is reflected from the mirror and collected by a diode at approximately $2\beta \sim 90°$ with respect to the incoming light. To measure polarization, the mirror is rotated around the beam axis z, parametrized by the angle ϕ. The polarization state of the reflected wave from the mirror is then given by

$$\boldsymbol{S}' = \mathcal{M}(\beta, h\nu)\mathcal{R}(\phi)\boldsymbol{S} \, ,$$

and the intensity detected by the diode is [39]

$$S_0^f = |r_p|^2 S_0 + \frac{1}{2}(|r_s|^2 - |r_p|^2)(S_0 + S_1\cos(2\phi) + S_2\sin(2\phi)) \, . \quad (9)$$

This quantity is solely a function of the initial Stokes parameters S_0, S_1 and S_2, which reflects the loss of phase information in the measurement process. A characterization of the circular polarization components S_3 with this type of polarimeter is therefore impossible without further assumptions. However, one can write S_3 in terms of the total degree of polarization Π

$$S_3 = \pm\sqrt{\Pi^2 S_0^2 - S_1^2 - S_2^2} \, . \quad (10)$$

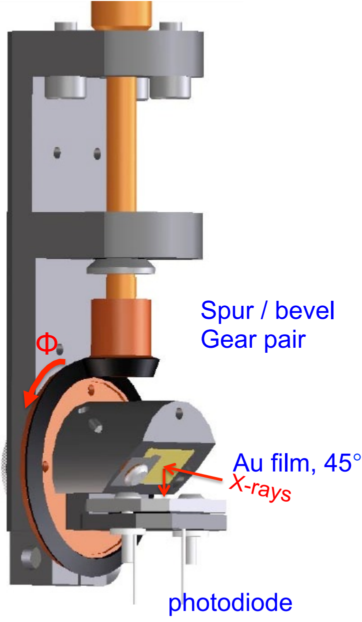

FIG. 7. Model of the reflective polarimeter used at MAESTRO. Design and implementation by David Kilcoyne.

pol	$\frac{EPU_z}{\text{mm}}$	S_0	$\frac{S_1}{S_0}$	$\frac{S_2}{S_0}$	$\frac{\|S_3\|_{\text{real}}}{S_0}$	$\frac{\|S_3\|_{\text{max}}}{S_0}$	Π_{min}	A	B	θ (°)
LV	-35.0	1.00	-0.82	-0.04	0.12	0.57	0.82	0.93	0.21	-88.63
	-30.0	1.35	-0.44	0.06	0.70	0.89	0.45	0.82	0.48	86.10
	-27.5	1.59	-0.21	0.08	0.80	0.98	0.22	0.75	0.59	79.93
LC	-25.0	1.76	-0.02	0.09	0.83	1.00	0.09	0.71	0.64	52.65
	-22.5	1.79	0.13	0.09	0.82	0.99	0.15	0.73	0.62	17.01
	-20.0	1.72	0.27	0.08	0.78	0.96	0.29	0.77	0.56	8.53
	-15.0	1.52	0.52	0.07	0.64	0.85	0.53	0.85	0.44	3.83
	-10.0	1.37	0.70	0.05	0.45	0.71	0.70	0.90	0.33	2.05
	-5.0	1.31	0.80	0.03	0.22	0.59	0.80	0.93	0.23	0.91
LH	0.00	1.31	0.83	0.00	0.00	0.55	0.83	0.93	0.20	-0.01
	5.0	1.31	0.79	-0.03	0.25	0.61	0.79	0.92	0.24	-0.93
	10.0	1.44	0.69	-0.05	0.46	0.72	0.69	0.90	0.33	-2.26
	15.0	1.64	0.51	-0.08	0.66	0.86	0.51	0.84	0.45	-4.53
	17.5	1.75	0.39	-0.09	0.73	0.91	0.40	0.81	0.50	-6.65
	20.0	1.85	0.26	-0.10	0.79	0.96	0.28	0.77	0.56	-10.71
	22.5	1.93	0.12	-0.11	0.82	0.99	0.16	0.73	0.61	-21.29
RC	25.0	1.84	-0.03	-0.12	0.82	0.99	0.12	0.72	0.63	-53.12
	27.5	1.64	-0.22	-0.12	0.79	0.97	0.25	0.76	0.58	-75.76
	30.0	1.35	-0.46	-0.12	0.68	0.88	0.48	0.83	0.47	-82.71
LV	35.0	1.00	-0.81	-0.06	0.18	0.58	0.81	0.93	0.22	-87.94

TABLE III. MAESTRO: Best fit values for the Stokes parameters at $h\nu = 100$ eV. The fit error is given by the last significant digit.

pol	$\frac{EPU_z}{\text{mm}}$	S_0	$\frac{S_1}{S_0}$	$\frac{S_2}{S_0}$	$\frac{\|S_3\|_{\text{real}}}{S_0}$	$\frac{\|S_3\|_{\text{max}}}{S_0}$	Π_{min}	A	B	θ (°)
LV	-45	1.00	-0.74	-0.02	0.40	0.67	0.74	0.91	0.30	-89.08
LC	-32.5	1.24	-0.09	-0.20	0.81	0.98	0.22	0.75	0.59	-56.51
LH	0	1.03	0.84	0.00	0.01	0.54	0.84	0.94	0.20	-0.01
RC	32.5	1.27	-0.09	0.20	0.81	0.98	0.22	0.75	0.59	57.35
LV	45	1.02	-0.75	0.02	0.38	0.67	0.75	0.91	0.29	89.31

TABLE IV. MERLIN: Best fit values for the Stokes parameters at $h\nu = 90$ eV. The fit error is given by the last significant digit.

Since $0 \leq \Pi \leq 1$ and the Stokes parameters are necessarily real, i.e. the argument of the square root must be positive, one finds a lower limit for the degree of polarization

$$\Pi_{\text{min}} = \sqrt{\frac{S_1^2 + S_2^2}{S_0^2}} \leq \Pi \leq 1\,, \tag{11}$$

which corresponds exactly to the degree of linear polarized light $\Pi_{\text{lin}} \equiv \Pi_{\text{min}}$.

In the experiment, the polarimeter was slightly tilted with respect to the z-axis. To fit the polarimeter data, a slight angle in between the rotation axis of the polarimeter and the beam axis is thus taken into account, described by $\beta \to \beta + \rho \sin(\phi + \zeta)$, where ρ describes the tilt angle and ζ describes the tilt direction with respect to the x-axis. In order to find these geometrical parameters, a fit of the polarimeter data for the EPU state that is known with certainty is made, i.e. the LH polarization configuration $EPU_z = 0$. In addition, all angle parameters are assumed to be close to the ideal ones ($\beta = 45°$, $\rho = 0$ and $\zeta = 0$), and within $\pm 1°$. The Stokes parameters S_0, S_1 and S_2 are left unconstrained.

Fits of LH polarization data obtained at MAESTRO for 100 eV photon energy, i.e. a typical energy used for ARPES measurements, are shown in the top left panel of Fig. 8. The alignment angles were found to be $\beta = 44°$, $\rho = -0.93°$ and $\zeta = 60.54°$, assumed as fixed for all further fits. The best fits for LV, RC and LC polarized light are shown in the remaining top panels. Table III summarizes the Stokes parameters S_0, S_1 and S_2 for polarizations obtained from continuously tuning the EPU phase EPU_z. These values can now be used to calculate the degree of linear polarization Π_{lin}, which at the same time corresponds to a lower estimate Π_{min} of the total degree of polarization. Assuming the total degree of polarization $\Pi = 1$, this gives an upper estimate for $|S_3|_{\text{max}}$, i.e. the maximum degree of circular polarization.

Clearly, the highest certainty of the polarization state is obtained for linear polarized light, with $\Pi \geq \Pi_{\text{lin}} = 83$ %. The lowest certainty is obtained for the circular polarized light, as the polarimeter is fundamentally unable to discriminate between circular and unpolarized light components. Assuming that the overall degree of polarization Π produced by the EPU does not significantly depend on the row phase EPU_z, a lower bound of the total degree of polarization can be estimated $\Pi \geq \Pi_{\text{lin}}(EPU_z = 0) \sim 83$ %, and a more realistic value $|S_3|_{\text{real}}$ can be calculated. The same consideration can be used to calculate the major and minor axis parameters A and B as well as the orientation θ of the polarization ellipse. A graphic representation of all fit results as a function of EPU_z is shown in Fig. 9. Under proper operation of the EPU, S_3 has to continuously change sign at $EPU_z = 0$. Hence, S_3 has to be identical zero at $EPU_z = 0$, which is indeed observed for $|S_3|_{\text{real}}$. The remaining 17 % of light thus result from depolarized light components, mostly introduced by the higher order EPU harmonics (at MAESTRO ~ 15 %, estimated from photoemission), and are thus not very relevant for the photoemission experiment.

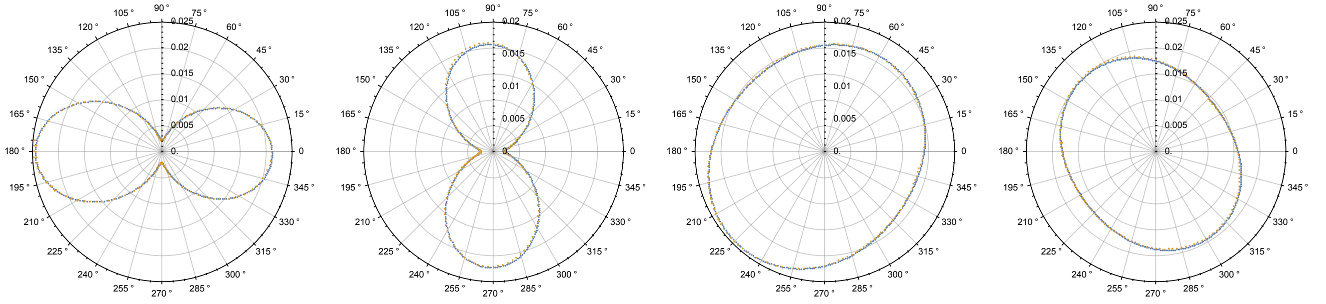

FIG. 8. Polarization fit of the linear horizontal (LH), the linear vertical (LV), the right circular (RC) and the left circular (LC) polarized light at $h\nu = 100$ eV. The angular acceptance of the beamline was set to 0.8 mrad. Yellow: data; Blue: fit.

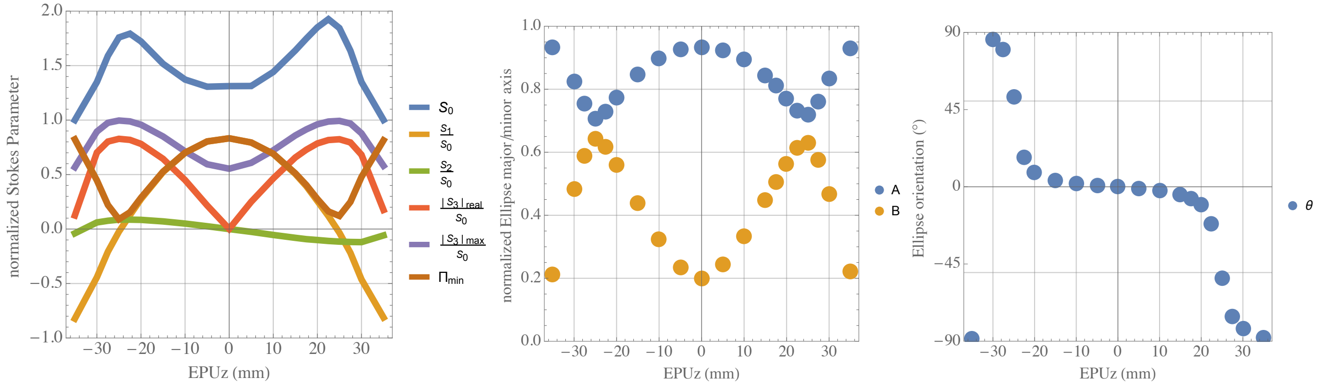

FIG. 9. MAESTRO: (left) Fit of Stokes parameters S_0, S_1 and S_2. Additionally, an upper estimate $|S_3|_{\text{max}}$ for a hypothetical $\Pi = 1$, and $|S_3|_{\text{real}}$ for a more realistic estimate of $\Pi \sim \Pi_{\text{min}}(EPU_z = 0) \sim 0.83$ are given. Further, a lower estimate of the degree of polarization Π_{min} is given. (Middle) Major axis A, minor axis B and (right) orientation angle θ (right) of the polarization ellipse calculated for $\Pi \sim \Pi_{\text{min}}(EPU_z = 0) \sim 0.83$.

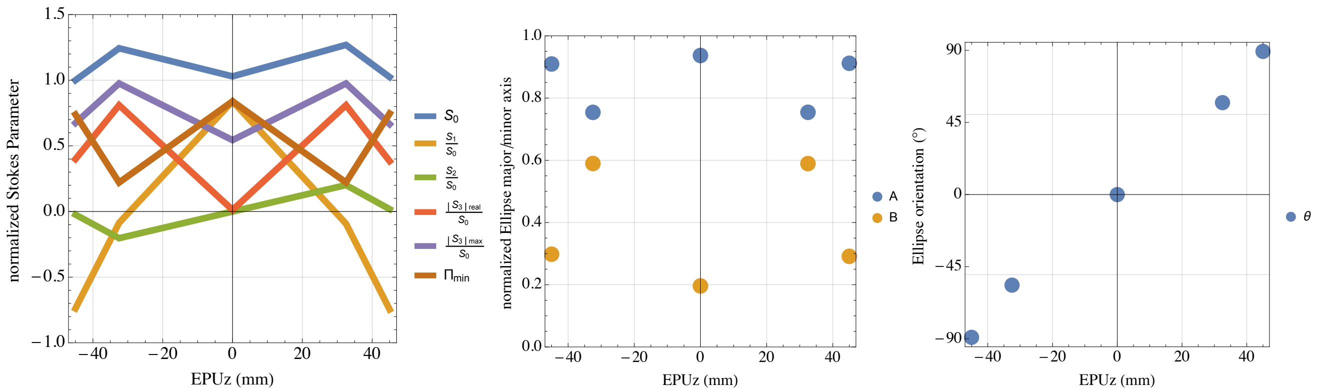

FIG. 10. MERLIN: (left) Fit of Stokes parameters S_0, S_1 and S_2. Additionally, an upper estimate $|S_3|_{\text{max}}$ for a hypothetical $\Pi = 1$, and $|S_3|_{\text{real}}$ for a more realistic estimate of $\Pi \sim \Pi_{\text{min}}(EPU_z = 0) \sim 0.84$ are given. Further, a lower estimate of the degree of polarization Π_{min} is given. (Middle) Major axis A, minor axis B and (right) orientation angle θ (right) of the polarization ellipse calculated for $\Pi \sim \Pi_{\text{min}}(EPU_z = 0) \sim 0.84$.

To compare with our results obtained at MAESTRO, a similar analysis was performed on polarization data obtained at the MERLIN photoemission beamline 4.0.3 of the Advanced Light Source. A summary of the fit results is given in Table IV and Fig. 10. Similar to the value obtained at MAESTRO, an estimate of the overall degree of polarization at MERLIN is

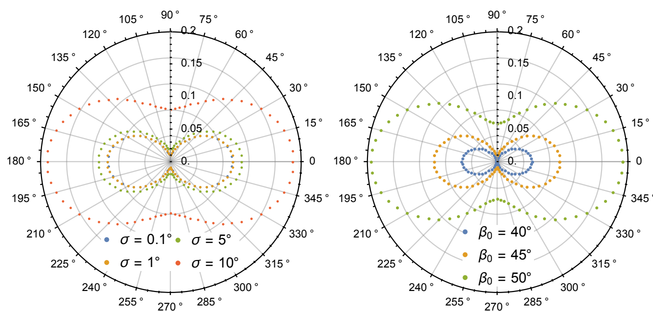

FIG. 11. (left) Effect of the beam divergence on the polarimeter output. (right) Effect of the scattering angle on the polarimeter output.

on the order of 84 %.

Both at MAESTRO and at MERLIN, the standard circular polarization states RC and LC are contaminated by linear polarized light contributions S_1 and S_2 well on the order of 10 %, introducing significant artifacts of linear dichroism to circular dichroism data. In a similar way, the linear polarization state LV contains sizable contributions of S_2 and S_3, potentially obscuring the interpretation of linear dichroism ARPES experiments. Depending on the exact status of the synchrotron storage ring, the EPU insertion device as well as the parameters of the beamline, the exact polarization state and its parasitic light components can fluctuate throughout time, and thus do not represent an absolute reference. To properly account for polarization artifacts, it is hence recommended to measure the polarization state under the same experimental conditions and close in time to the actual ARPES experiment. As the polarimeter at MAESTRO is fully automated, such polarization data can be acquired in only a few minutes.

Finally, the robustness of our analysis with respect to the X-ray beam divergence $\sigma \sim 1^\circ$ at MAESTRO, i.e. its influence on the observed polarimeter output, is tested. Assuming that the angular distribution of the incoming light follows a Gaussian profile $\sim 1/\sigma \; e^{(\beta-\beta_0)^2/\sigma^2}$ around the scattering angle $\beta_0 = 45^\circ$, the total intensity on the polarimeter is calculated as

$$I_{\text{tot}} = \frac{1}{\sigma} \int_0^{\pi/2} \frac{\partial I}{\partial \beta} e^{(\beta-\beta_0)^2/\sigma^2} d\beta \; . \tag{12}$$

Plots for varying σ are shown in Fig. 11. Up to $\sigma \sim 5^\circ$, the divergence of the beam has only a small effect on the polarization measurement. Above this value, it produces a considerable waist. In a similar way, note that the alignment of the polarimeter, given by the scattering angle β_0, would produce a waist for β significantly deviating from 45°. At MAESTRO, both σ and β_0 are within 1° of their nominal values and thus do not affect the polarimeter output significantly.

CONCLUSION

In conclusion, this work discusses polarization control at the new MAESTRO photoemission beamline at the ALS in Berkeley. Numerical simulations show that the degree of polarization produced by the EPU can be tuned up to 100 % for the first harmonics if the angular acceptance of the beamline selects mostly on axis radiation. Phase retardation at the downstream optical components of the beamline, in particular the monochromator assembly, introduce significant and photon energy dependent changes in the polarization, but leave the degree of polarization mostly unaffected. Characterizing the polarization by a simple reflective polarimeter in proximity to the downstream experimental end-station yields a total degree of polarization of $\sim$ 83 % at 100 eV photon energy, with the remaining 17 % mostly resulting from depolarized higher order EPU harmonics. All common linear and circular polarization states contain parasitic polarization components to be taken into account in the interpretation of the ARPES data. In particular, a proper characterization of polarization alongside with the actual ARPES experiment is recommended to discern intrinsic dichroism effects from artifacts introduced by improper polarization. This work presents the necessary tool-set to characterize the polarization state at MAESTRO, and simplistic routes towards polarization assessment at synchrotron light sources elsewhere.

ACKNOWLEDGEMENTS

We thank Erik Wallén, Joshua Machacek and Jessee Liberty Freeman for helpful input and support. S.M. acknowledges support by the Swiss National Science Foundation under Grant No. P2ELP2-155357. This research used resources of the Advanced Light Source, which is a US Department of Energy Office of Science User Facility under contract no. DE-AC02-05CH11231.

[1] H. ONUKI, Undulators, Wigglers and their Applications, edited by H. Onuki and P. Elleaume (Taylor & Francis, Abingdon, UK, 2003) p. 214.

[2] N. Böwering, T. Lischke, B. Schmidtke, N. Müller, T. Khalil, and U. Heinzmann, Physical Review Letters **86**, 1187 (2001).

[3] T. Jahnke, T. Weber, A. L. Landers, A. Knapp, S. Schössler, J. Nickles, S. Kammer, O. Jagutzki, L. Schmidt, A. Czasch, T. Osipov, E. Arenholz, A. T. Young, R. Díez Muiño, D. Rolles, F. J. García de Abajo, C. S. Fadley, M. A. Van Hove, S. K. Semenov, N. A. Cherepkov, J. Rösch, M. H. Prior, H. Schmidt-Böcking, C. L. Cocke, and R. Dörner, Physical Review Letters **88**, 073002 (2002).

[4] Y. H. Wang, D. Hsieh, D. Pilon, L. Fu, D. R. Gardner, Y. S. Lee, N. Gedik, I. Si, S. I. Ii, and V. Si, Physical Review Letters **107**, 1 (2011), arXiv:arXiv:1101.5636v2.

[5] Y. Liu, G. Bian, T. Miller, and T.-C. Chiang, Physical Review Letters **107**, 166803 (2011).

[6] S. R. Park, J. Han, C. Kim, Y. Y. Koh, C. Kim, H. Lee, H. J. Choi, J. H. Han, K. D. Lee, N. J. Hur, M. Arita, K. Shimada, H. Namatame, and M. Taniguchi, Physical Review Letters **108**, 046805 (2012).

[7] M. Lebech, J. C. Houver, G. Raseev, A. S. dos Santos, D. Dowek, and R. R. Lucchese, The Journal of Chemical Physics **136**, 094303 (2012).

[8] M. Ärrälä, J. Nieminen, J. Braun, H. Ebert, and M. Lindroos, Physical Review B **88**, 195413 (2013).

[9] G. Bian, L. Zhang, Y. Liu, T. Miller, and T.-C. Chiang, Physical Review Letters **108**, 186403 (2012).

[10] Z.-H. Zhu, C. N. Veenstra, G. Levy, A. Ubaldini, P. Syers, N. P. Butch, J. Paglione, M. W. Haverkort, I. S. Elfimov, and A. Damascelli, Physical Review Letters **110**, 216401 (2013).

[11] J. Sánchez-Barriga, A. Varykhalov, J. Braun, S.-Y. Xu, N. Alidoust, O. Kornilov, J. Minár, K. Hummer, G. Springholz, G. Bauer, R. Schumann, L. V. Yashina, H. Ebert, M. Z. Hasan, and O. Rader, Physical Review X **4**, 011046 (2014).

[12] L. Nahon, G. A. Garcia, and I. Powis, Journal of Electron Spectroscopy and Related Phenomena **204**, 322 (2015).

[13] H. Bentmann, H. Maaß, E. E. Krasovskii, T. R. F. Peixoto, C. Seibel, M. Leandersson, T. Balasubramanian, and F. Reinert, Physical Review Letters **119**, 106401 (2017), arXiv:1507.04664.

[14] S. Moser, Journal of Electron Spectroscopy and Related Phenomena **214**, 29 (2017).

[15] T. Koide, T. Shidara, M. Yuri, N. Kandaka, K. Yamaguchi, and H. Fukutani, Nuclear Instruments and Methods in Physics Research Section A: Accelerators, Spectrometers, Detectors and Associated Equipment **308**, 635 (1991).

[16] H. Petersen, M. Willmann, F. Schäfers, and W. Gudat, Nuclear Instruments and Methods in Physics Research Section A: Accelerators, Spectrometers, Detectors and Associated Equipment **333**, 594 (1993).

[17] T. Koide, T. Shidara, and M. Yuri, Nuclear Instruments and Methods in Physics Research Section A: Accelerators, Spectrometers, Detectors and Associated Equipment **336**, 368 (1993).

[18] F. Schäfers, H.-C. Mertins, A. Gaupp, W. Gudat, M. Mertin, I. Packe, F. Schmolla, S. Di Fonzo, G. Soullié, W. Jark, R. Walker, X. Le Cann, R. Nyholm, and M. Eriksson, Applied Optics **38**, 4074 (1999).

[19] M. Weiss, R. Follath, K. Sawhney, F. Senf, J. Bahrdt, W. Frentrup, A. Gaupp, S. Sasaki, M. Scheer, H.-C. Mertins, D. Abramsohn, F. Schäfers, W. Kuch, and W. Mahler, Nuclear Instruments and Methods in Physics Research Section A: Accelerators, Spectrometers, Detectors and Associated Equipment **467-468**, 449 (2001).

[20] L. Nahon and C. Alcaraz, Applied Optics **43**, 1024 (2004).

[21] P. Finetti, D. Holland, C. Latimer, and C. Binns, Nuclear Instruments and Methods in Physics Research Section B: Beam Interactions with Materials and Atoms **215**, 565 (2004).

[22] J. Bahrdt, R. Follath, W. Frentrup, A. Gaupp, M. Scheer, R. Garrett, I. Gentle, K. Nugent, and S. Wilkins, in AIP Conference Proceedings, Vol. 1234 (2010) pp. 335–338.

[23] H. Wang, P. Bencok, P. Steadman, E. Longhi, J. Zhu, and Z. Wang, Journal of Synchrotron Radiation **19**, 944 (2012).

[24] L. Nahon, N. de Oliveira, G. A. Garcia, J.-F. Gil, B. Pilette, O. Marcouillé, B. Lagarde, and F. Polack, Journal of Synchrotron Radiation **19**, 508 (2012).

[25] S. Uschakow, A. Gaupp, M. Gerhard, M. MacDonald, and F. Schäfers, Nuclear Instruments and Methods in Physics Research Section A: Accelerators, Spectrometers, Detectors and Associated Equipment **710**, 120 (2013).

[26] S. Yamamoto, Y. Senba, T. Tanaka, H. Ohashi, T. Hirono, H. Kimura, M. Fujisawa, J. Miyawaki, A. Harasawa, T. Seike, S. Takahashi, N. Nariyama, T. Matsushita, M. Takeuchi, T. Ohata, Y. Furukawa, K. Takeshita, S. Goto, Y. Harada, S. Shin, H. Kitamura, A. Kakizaki, M. Oshima, and I. Matsuda, Journal of Synchrotron Radiation **21**, 352 (2014).

[27] R. C. Jones, Journal of the Optical Society of America **31**, 488 (1941).

[28] W. B. Westerveld, K. Becker, P. W. Zetner, J. J. Corr, and J. W. McConkey, Applied Optics **24**, 2256 (1985).

[29] S. Chwirot, S. N. Chormaic, D. Dziczek, and J. Slevin, Applied Optics **32**, 1583 (1993).

[30] J. Schwinger, Physical Review **75**, 1912 (1949).

[31] K. C. Westfold, The Astrophysical Journal **130**, 241 (1959).

[32] T. Tanaka and H. Kitamura, Journal of Synchrotron Radiation **8**, 1221 (2001).

[33] T. Warwick, LSBL 1037RevB: MAESTRO Beam Line Implementation and S Tech. Rep. (Advanced Light Source, Berkeley, 2012).

[34] S. Sasaki, I. McNulty, and R. Dejus, Nuclear Instruments and Methods in Physics Research, Section A: Accelerators, Spectrometers, Detectors and Associated Equipment **582**, 43 (2007).

[35] S. Sasaki and I. McNulty, Physical Review Letters **100**, 1 (2008).

[36] J. Bahrdt, K. Holldack, P. Kuske, R. Müller, M. Scheer, and P. Schmid, Physical Review Letters **111**, 034801 (2013).

[37] G. Rosenbaum, B. Feuerbacher, R. P. Godwin, and M. Skibowski, Applied Optics **7**, 1917 (1968).

[38] W. R. Hunter, Applied Optics **17**, 1259 (1978).

[39] S. Zuccon, M.-g. Pelizzo, P. Nicolosi, A. Giglia, N. Mahne, and S. Nannarone, in Proc. SPIE 7077, Advances in X-Ray/EUV Optics and Components III, Vol. 7077, edited by S. Goto, A. M. Khounsary, and C. Morawe (2008) p. 70771R.

[40] D. W. Berreman, Journal of the Optical Society of America **62**, 502 (1972).

[41] L. Li, Journal of the Optical Society of America A **13**, 1870 (1996).

[42] L. Li, Journal of the Optical Society of America A **13**, 1024 (1996).

[43] M. G. Moharam and T. K. Gaylord, Journal of the Optical Society of America **71**, 811 (1981).

[44] M. G. Moharam and T. K. Gaylord, Journal of the Optical Society of America **72**, 1385 (1982).

[45] K. Rokushima and J. Yamakita, Journal of the Optical Society of America **73**, 901 (1983).

[46] L. Doskolovich, E. Kadomina, I. Kadomin, and S. Kharitonov, Optical Memory and Neural Networks **16**, 24 (2007).

[47] R. M. A. Azzam, Applied Optics **31**, 3574 (1992).

[48] R. M. A. Azzam and K. A. Giardina, Journal of the Optical Society of America A **10**, 1190 (1993).

[49] S. Krishnan, S. Hampton, J. Rix, B. Taylor, and R. M. a. Azzam, Applied Optics **42**, 1216 (2003).

[50] Y. Otani, T. Kuwagaito, Y. Mizutani, and N. Umeda, SEM Annual Conference & Exposition on Experimental and Applied Mechanics , 1 (2007).

[51] Y. Otani, Evaluation , 1 (2009).

[52] M. Foldyna, A. De Martino, R. Ossikovski, E. Garcia-Caurel, and C. Licitra, Optics Communications **282**, 735 (2009).

[53] M. Foldyna, A. De Martino, C. Licitra, J. Foucher, and S. Ben Hatit, EPJ Web of Conferences **5**, 02003 (2010).

[54] T. Novikova, P. Bulkin, V. Popov, B. Haj Ibrahim, and A. De Martino, Journal of Vacuum Science & Technology B: Microelectronics and Nanometer Structures **29**, 051804 (2011).

[55] R. M. A. Azzam, Journal of the Optical Society of America A **33**, 1396 (2016).
[56] S. Fujiwara and Y. Iguchi, Journal of the Optical Society of America **58**, 1189 (1968).
[57] H. Padmore, V. Martynov, and K. Holis, Nuclear Instruments and Methods in Physics Research Section A: Accelerators, Spectrometers, Detectors and Associated Equipment **347**, 206 (1994).
[58] T. Kachel, F. Eggenstein, and R. Follath, Journal of Synchrotron Radiation **22**, 1301 (2015).
[59] B. Henke, E. Gullikson, and J. Davis, Atomic Data and Nuclear Data Tables **54**, 181 (1993).
[60] M. Foldyna, A. De Martino, R. Ossikovski, E. Garcia-Caurel, and C. Licitra, Optics Communications **282**, 735 (2009).
[61] T. Saito, K. Ozaki, K. Fukui, H. Iwai, K. Yamamoto, H. Miyake, and K. Hiramatsu, Thin Solid Films **571**, 517 (2014).
[62] H. Daimon, T. Nakatani, S. Imada, S. Suga, Y. Kagoshima, and T. Miyahara, Review of Scientific Instruments **66**, 1510 (1995).
[63] K. Veyrinas, C. Elkharrat, S. Marggi Poullain, N. Saquet, D. Dowek, R. R. Lucchese, G. A. Garcia, and L. Nahon, Physical Review A **88**, 063411 (2013).
[64] E. Allaria, B. Diviacco, C. Callegari, P. Finetti, B. Mahieu, J. Viefhaus, M. Zangrando, G. De Ninno, G. Lambert, E. Ferrari, J. Buck, M. Ilchen, B. Vodungbo, N. Mahne, C. Svetina, C. Spezzani, S. Di Mitri, G. Penco, M. Trovó, W. M. Fawley, P. R. Rebernik, D. Gauthier, C. Grazioli, M. Coreno, B. Ressel, A. Kivimäki, T. Mazza, L. Glaser, F. Scholz, J. Seltmann, P. Gessler, J. Grünert, A. De Fanis, M. Meyer, A. Knie, S. P. Moeller, L. Raimondi, F. Capotondi, E. Pedersoli, O. Plekan, M. B. Danailov, A. Demidovich, I. Nikolov, A. Abrami, J. Gautier, J. Lüning, P. Zeitoun, and L. Giannessi, Physical Review X **4**, 041040 (2014).
[65] K. Rabinovitch, L. R. Canfield, and R. P. Madden, Applied Optics **4**, 1005 (1965).
[66] J. A. R. Samson, Review of Scientific Instruments **47**, 859 (1976).
[67] E. S. Gluskin, Review of Scientific Instruments **63**, 1523 (1992).